Mitigation of Cross-Beam Energy Transfer in Symmetric Implosions on OMEGA Using Wavelength Detuning

Introduction

In the direct-drive[1,2] approach to inertial confinement fusion (ICF), laser beams directly illuminate a spherical target, depositing most of their energy in the coronal plasma. This energy is transported by electron thermal conduction through a conduction zone to higher densities, where ablation occurs. At the ablation surface, material rapidly expands, producing pressure that drives the shell of the target and thermonuclear fuel [usually deuterium–tritium (DT)] toward the center of the capsule, compressing the target to ~400 g/cm^3 (Ref. 2). To achieve this compression, the laser pulses are precisely shaped to launch a series of synchronized spherical shocks that cause the fuel to compress quasi-adiabatically. As the capsule converges, its kinetic energy is converted to internal energy, creating a hot dense core in which fusion reactions initiate, surrounded by a cold, dense, nearly Fermi-degenerate shell.[1–3]

Successful direct-drive ignition requires both efficient deposition of the laser energy in the coronal plasma and uniform target illumination to produce the spherically symmetric drive required to avoid hydrodynamic instabilities and low-mode-number asymmetries that can quench the implosion.[4,5] The target is illuminated by a number of beams, distributed symmetrically around the target, with diameters that are selected by the trade-off between increased drive uniformity and decreased drive efficiency as the laser spot size increases.[6] When neglecting laser–plasma instabilities, a laser focal-spot radius approximately equal to the target radius provides the best compromise.[7]

The total laser drive pressure and its uniformity can be significantly degraded by the transfer of energy between laser beams crossing in the coronal plasma.[8–12] Cross-beam energy transfer (CBET) is a three-wave process that occurs when the beat wave created by the interference between two electromagnetic waves resonantly excites a plasma ion-acoustic wave (IAW) as shown in Fig. 150.11. When two lasers with frequencies ω_1, ω_2 and wave vectors $\vec{k}_1$, $\vec{k}_2$ cross in a plasma, the ponderomotive force of their beat wave can drive a plasma density perturbation. These density perturbations form a grating and cause Bragg diffraction, facilitating the transfer via stimulated Brillouin scattering (SBS). The coupling is maximized when the driven wave satisfies the dispersion relation for the IAW:

$$\omega_{\mathrm{IAW}} - \vec{u}_{\mathrm{f}} \cdot \vec{k}_{\mathrm{IAW}} = \pm c_{\mathrm{s}} \left| k_{\mathrm{IAW}} \right|,$$

$$\omega_{\mathrm{IAW}} = \omega_1 - \omega_2, \tag{1}$$

$$\vec{k}_{\mathrm{IAW}} = \vec{k}_1 - \vec{k}_2,$$

where $\vec{u}_{\mathrm{f}}$ is the local plasma hydrodynamic flow velocity, c_{s} is the local sound speed, and ω_{IAW} and $\vec{k}_{\mathrm{IAW}}$ are the frequency and wave vector, respectively, of the ion-acoustic wave. The two branches $\left(\pm c_{\mathrm{s}} \left| k_{\mathrm{IAW}} \right|\right)$ of the dispersion relation correspond to the direction of power flow from the higher-frequency (in the plasma reference frame) "pump" wave to the lower-frequency "seed" wave. Since CBET is seeded by a laser beam rather than small-amplitude thermal noise, significant energy can be exchanged even when the SBS gain is small.

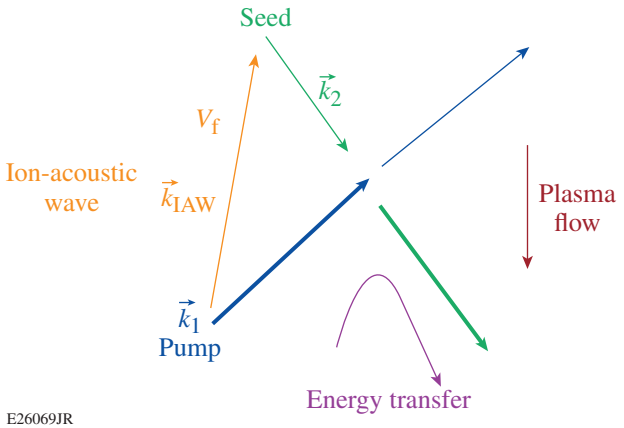

Figure 150.11
A k-space diagram of cross-beam energy transfer (CBET). Energy is transferred from the pump beam to the seed beam as indicated by the magenta arrow labeled "Energy transfer."

Experiments have demonstrated the existence of CBET between frequency-mismatched beams[13] and beams with the same frequency but crossing in a flowing plasma.[14–18] CBET has been modeled many times for a pair of crossing beams.[19–22] Indirect-drive hohlraum experiments at the National Ignition Facility (NIF)[23] have identified CBET as a mechanism responsible for transferring significant amounts of energy between laser beams.[24] In these experiments, the angle between crossing beams was small enough that steady-state CBET models could use a 3-D paraxial approximation or neglect small 3-D effects.

These models showed that significant CBET occurred between NIF beams when they were at the same wavelength and that energy was forward scattered from beams pointed toward the hohlraum equator to those directed nearer to the ends of the hohlraum, affecting the implosion symmetry on indirect-drive hohlraum experiments. It was also shown that CBET can distort the effective beam profile[20] even when the net transfer between beams is zero.[25] These models predicted that relatively small wavelength shifts (of the order of 1 Å) could tune the shape of an indirect-drive hohlraum implosion by transferring energy between beam rings. Independently varying the wavelength of the NIF beams to control CBET is now used as a tool to tune the implosion symmetry on the NIF[25–29] and to reduce stimulated Raman scattering (SRS) backscatter.[27,30] Recently, an in-line CBET model[31,32] was incorporated into the main 3-D radiation–hydrodynamics code, known as *HYDRA*,[33] for the NIF.

In direct drive, the presence of CBET was first inferred from the experimental observation of the scattered-light spectra[34,35] and the implosion velocity.[36,37] Early direct-drive CBET modeling typically used a 1-D linear geometry;[10,38] however, to properly model a direct-drive implosion, the crossings of many beams must be calculated simultaneously. The complex beam paths caused by refraction through the coronal plasma invalidate the paraxial approximation, and CBET models for direct-drive implosions typically use 3-D ray tracing to calculate the crossing beam trajectories. Initial CBET modeling suggested that in direct drive, CBET could backscatter energy out of ingoing rays from the hydrodynamically efficient small-impact parameter inner portion of the laser beam spot to outgoing large-impact parameter rays near the edge of the beam spot.[34,39] This would allow significant amounts of the incident energy from the central portion of the laser beams to bypass the highest absorption region near the critical surface, reducing the ablation pressure and hydrodynamic efficiency of the implosion. The redistribution of power modifies the effective beam profile identically for each beam in a symmetric implosion and can have a large effect on a target's illumination uniformity. The details and orientation of the redistribution depend on the 3-D positions of the beams with respect to each other and should be modeled in 3-D. In-line ray-based CBET models[36,40,41] have now been added to the direct-drive codes *LILAC* (1-D)[42] and *DRACO* (2-D),[43] which allow one to hydrodynamically self-consistently model CBET in direct-drive implosions. CBET redistributes ~30% of the incident energy on OMEGA at intensities of 5×10^{14} W/cm^2 and is responsible for a 10% to 20% reduction in laser absorption according to the *LILAC* model.[36]

Several different schemes have been proposed to mitigate CBET in direct-drive implosions, including doped ablators,[40] narrow beams,[36,44–46] and multicolor lasers.[36,40] The predictions in direct drive that outgoing light from the edge of the beam was taking energy out of the incoming light from the beam center led to the proposal that shrinking the beam radius would reduce CBET.[36] Studies have shown that reducing the diameter of the laser beams by 30% can restore nearly all of the kinetic energy lost to CBET, but at a cost of increased low-mode perturbations.[44] Low-mode uniformity might be maintained by using two-state beam "zooming," where the implosion is initiated using full-sized beams that are then reduced in radius after the corona has developed a sufficient conduction zone to smooth out perturbations.[45] Implementing zooming on OMEGA would require new phase plates, referred to as zooming phase plates (ZPP's) and co-propagating dual driver lines.[46] Using laser beams with multiple wavelengths has been proposed to mitigate CBET in direct-drive implosions. Color-splitting the beams into two or more co-propagating wavelengths with $\Delta\lambda >$ 5 Å reduces CBET by ~50% in 1-D modeling.[36,40] Instead of each beam containing multiple wavelengths, the beams could be grouped into subsets of monochromatic beams with distinct wavelengths.[47] The current in-line models will not capture the full effect of the 3-D beam distribution because of their respective 1-D and 2-D approximations.

In this article, the effects of frequency detuning laser beams in direct-drive symmetric implosions are studied using a 3-D CBET model. To our knowledge, this is the first fully 3-D modeling of CBET for direct-drive implosions. The 3-D ray-based CBET model was benchmarked against full-field calculations,[48] providing confidence in the implementation of the model to calculate the effects of CBET in full-scale implosion experiments. These calculations show that interactions between beams with relative angles between 45° and 90° are the most significant for CBET in OMEGA direct-drive implosions. Redistribution of laser power because of CBET can increase the rms (root mean square) absorption nonuniformity by an order

of magnitude. Shifting the relative wavelengths of three groups of laser beams by ~10 Å maximized the total absorption, and the rms absorption nonuniformity was near minimum for the implosion conditions studied in this article.

The following sections discuss the model equations and gridding; report on model results for two-beam and many-beam CBET coupling when all the beams are launched with the same wavelength; and present predictions for a CBET mitigation scheme in 60-beam symmetric OMEGA direct-drive implosions using wavelength detuning.

The 3-D CBET Model

The CBET model used here (*BeamCrosser*) was originally developed as a *MATLAB*[49]-based hydrodynamics code postprocessor to simulate scattered-light spectra from OMEGA implosions[50] and provided the first evidence that CBET was significantly degrading implosion performance relative to 1-D hydrodynamic predictions.[34,39] As a hydrodynamics code postprocessor, the CBET model relies on time-varying coronal plasma parameters calculated independently by a hydrodynamics code such as *LILAC* (1-D) or *DRACO* (2-D). The CBET model is used to gain insight into 3-D effects during an implosion, even though its calculations are not fully self-consistent with the plasma hydrodynamics.

1. Ray Tracing and Model Gridding

The model is a ray-based CBET model and therefore does not solve the full electromagnetic Maxwell equations. The reduced ray equation for geometric optics[51] is used to determine the laser beam propagation through the coronal plasma of an implosion. The ray equation is solved by a fourth-order Runge–Kutta method similar to that of Sharma *et al.*[52]

A single geometric optics-based ray is simply a path through space that by itself carries no inherent information about the local light intensity. The laser intensity along a ray is calculated using the intensity law of geometrical optics[51] and the spacing between points of neighboring rays on the same wavefront (having equal optical path lengths) along with the change in intensity caused by absorption and CBET, as discussed in the next section.

An example of the ray paths for a single laser beam propagating through a spherically symmetric coronal plasma of a direct-drive implosion is shown in Fig. 150.11. Refraction of the rays produces a paraboloid-like shadow behind the target inside of which rays cannot reach. The envelope of tangential rays defining the boundary surface of the shadow volume is a caustic[53] of the "fold catastrophe" type,[54] where rays fold upon themselves and all points on the unshadowed side of the caustic are intersected by two distinct rays. The points where the rays graze the caustic are sometimes referred to as their "turning points,"[53] but that is not true in general. The turning point is best defined as the point of deepest radial penetration into the coronal plasma. It is clear from the outermost rays shown in Fig. 150.12 that these rays cross well away from their closest approach to the target. The intensity law of geometrical optics breaks down near the caustic, where the spacing between points on the same wavefront becomes very small, giving unphysically high intensities. The actual intensity where two rays cross is limited by diffraction. The intensity near the caustic is similar to an Airy pattern superimposed on the intensity from the geometric law. The CBET model limits the intensity along the rays from reaching unphysically high intensities by using either a fixed limiting factor or a field swelling limit based on Kruer;[48,55] however, this limit has only a small effect on the results of the code since it is applied only in a small volume.

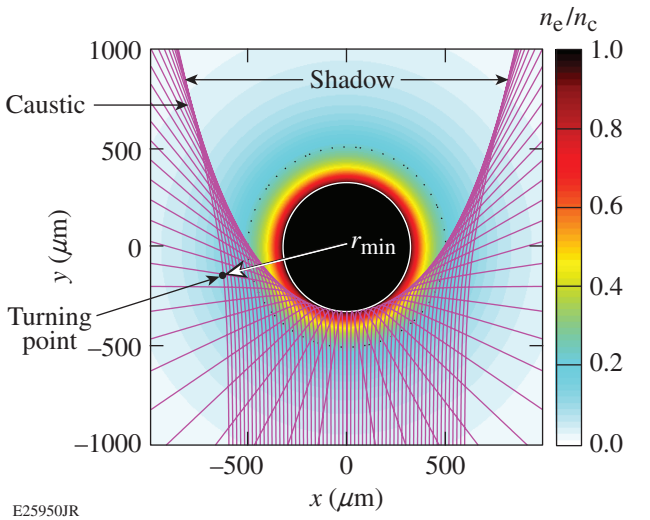

Figure 150.12
Ray tracing of a laser beam through a spherical plasma.

The change in local laser frequency along the ray path resulting from changing plasma conditions is calculated from the difference in flight times of successive wavefronts:[56]

$$\Delta\omega = \omega_L \frac{\partial \tau}{\partial t}, \tag{2}$$

where ω_L is the initial laser vacuum frequency and τ is flight time of the light along the ray. The rate of change in flight time is directly calculable along a ray using the local rate of change in plasma density along each ray path. Calculating this general-

ized Doppler effect is essential because the change in frequency between incoming and outgoing rays in a typical direct-drive implosion is of the same order as the difference in the frequency needed for CBET (approximately a few angstroms).

The model "gridding" follows the beam trajectories determined by the ray trace. Each on-target laser beam profile is discretized into many square "beamlets" with flat intensities on a 2-D grid, as shown in Fig. 150.13(a). The distance along the path of each beamlet provides the third dimension for the gridding of each beam. Figure 150.13(b) shows this non-orthogonal overlapping grid in which more than one cell for a single beam can occupy the same physical space. CBET at these intrabeam crossings between beamlets from the same beam is calculated by the model in addition to crossing between beamlets from different beams. The significant refraction of the laser light in a direct-drive implosion plasma is a major difference from indirect drive, where the refraction of the laser beams can typically be ignored[26] and the paraxial approximation can be employed[25] in the volume where the beams cross.

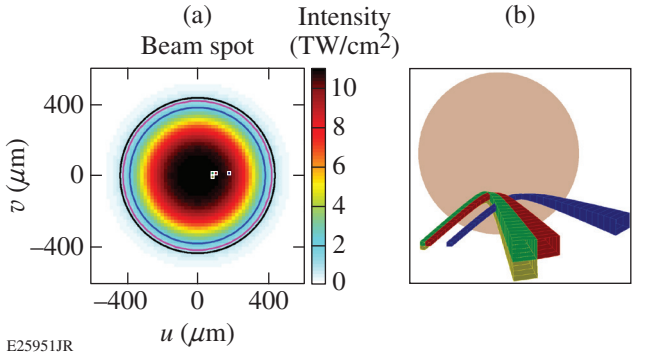

Figure 150.13
(a) Laser beam discretization into beamlets for an OMEGA beam with SG4 phase plates. The magenta circle is the nominal beam radius (contour containing 95% of the beam energy); (b) 3-D gridlines of four sample beamlets corresponding to the same-colored squares in (a).

2. CBET Theory and Equations

The CBET equations used in the model are a 3-D extension of the quasi-steady-state 1-D slab fluid model of Randall *et al.*,[38] which assumes that where two rays cross, they can be treated locally as plane waves. To facilitate conservation of energy, the equations are written in terms of power rather than intensity.

The total power in a beamlet P_b along its path (s) is followed by the model as

$$dP_b(s) = P_b(s)\left(\frac{1}{L_{abs}} + \sum_{\substack{\text{all beam}\\ \text{crossings}}} \frac{C_{CBET}}{L_{CBET}}\right)ds, \tag{3}$$

where L_{abs} is the scale length of inverse bremsstrahlung absorption.[57] C_{CBET} is a multiplier, typically of the order of 2 for implosion modeling,[58] applied to the calculated CBET coupling to better match experimental measurements (discussed in detail below). L_{CBET} is the local spatial rate of energy gain/loss because of CBET in the strong damping limit:[36,38,59]

$$L_{CBET}^{-1} = 5.85\times10^{-2}\frac{1}{\nu_a}\frac{n_e/n_c}{\left(1-n_e/n_c\right)} \times \frac{I_{14}\lambda_{0,\mu m}}{T_{e,keV}\left(1+3T_{i,keV}/ZT_{e,keV}\right)} \times \psi \times R(\eta)\left(\mu m^{-1}\right), \tag{4}$$

where $\lambda_{0,\mu m}$ is the laser wavelength in microns, I_{14} is the crossing laser intensity in 10^{14} W/cm^2, $T_{e,keV}$ and $T_{i,keV}$ are the electron and ion temperatures, respectively, in keV, Z is the average ionization, ν_a is the dimensionless amplitude damping rate for the IAW, n_e is the electron density, and n_c is the critical density. Since L_{CBET} depends on the intensity of the crossing beamlets, Eqs. (3) and (4) form a set of coupled nonlinear equations.

The factor $R(\eta)$ is the resonance function accounting for how closely the driven wave satisfies the IAW dispersion relation [Eq. (1)],

$$R(\eta) = \frac{\nu_a^2\eta}{\left(\eta^2-1\right)^2+\nu_a^2\eta^2}, \qquad \eta = \left(\vec{k}_{IAW}\cdot\vec{u}_f-\omega_{IAW}\right)/k_{IAW}c_s. \tag{5}$$

The factor ψ accounts for the effect of polarization on the coupling of the crossing beams. For random polarization or when the beams have their polarization evenly distributed in two orthogonal components,

$$\psi = \frac{1}{4}\left(1+\cos^2\theta_k\right), \tag{6}$$

where θ_k is the beam crossing angle.[60] This is appropriate for most implosions on OMEGA, where distributed polarization rotators (DPR's)[61] are used to split the beams into orthogonal polarizations, or on the NIF, where the beams are arranged in quads in such a way that the polarizations of two beams are orthogonal to the polarization of the other two beams in the quad.[60] When DPR's are not used on OMEGA, the beams are linearly polarized and the coupling between the beams affects only the shared polarization component.[62]

As mentioned above, outside the beam shadow, all points are crossed twice by rays from each beam, so there are a total of $2N-1$ possible crossings to be considered at each point along a beamlet, where N is the total number of beams. Equations (4)–(6) are applied to all beamlet crossings to determine the total CBET coupling at each grid point along all beamlets. Since pump depletion is inherent in CBET, the system is solved using fixed-point iteration. Energy is conserved by balancing the power exchanged between beamlets such that the power gain (loss) calculated for beamlet A where it is crossed by beamlet B is identical to the power loss (gain) for beamlet B where it is crossed by beamlet A.

3. Benchmarking the Model

The CBET model was benchmarked by comparing it with the predictions of a full-wave code *LPSE* (laser-plasma simulation environment).[48] *LPSE* solves the time-enveloped Maxwell equations coupled to a linearized time-dependent fluid plasma response to calculate the enveloped electric-field vector and the ponderomotively driven ion-density perturbations. *LPSE* is impractical for full-scale 3-D implosion modeling because of its computational costs, but full-scale 2-D and reduced-scale 3-D runs provide good benchmarks for a ray-based model.

Figure 150.14 shows an *LPSE* calculation of two lasers crossing in a constant-density plasma with a linearly varying plasma velocity profile that places the maximum of the resonance function [Eq. (2)] at $x = 8.6\ \mu$m. Both beams are polarized 45° out of the plane. CBET affects only the components of the polarization that are shared by the beams, so the polarization of each beam is expected to rotate. The intensities of the beams after undergoing CBET predicted by the ray-based model (with $C_{\mathrm{CBET}} = 1$) are an excellent match to those predicted by *LPSE* [Fig. 150.14(b)]. The predicted rotation in the polarization caused by CBET is very good over the region where the beam power is significant, but some divergence between the calculations is observed where the beam intensities are small. Overall, the comparison with the full-field calculations of *LPSE* provides confidence on the validity of the approximations made in the ray-based code.

In direct-drive implosions, experimental measurements of the ablation rate and the ablation-front trajectory on both OMEGA and the NIF are in good agreement with *DRACO* predictions provided a CBET gain multiplier of $C_{\mathrm{CBET}} = 2$ is used.[58] A similar factor of $C_{\mathrm{CBET}} = 2$ is required by the CBET model described here in order for its scattered-light predictions to match observations. This indicates that some physics pres-

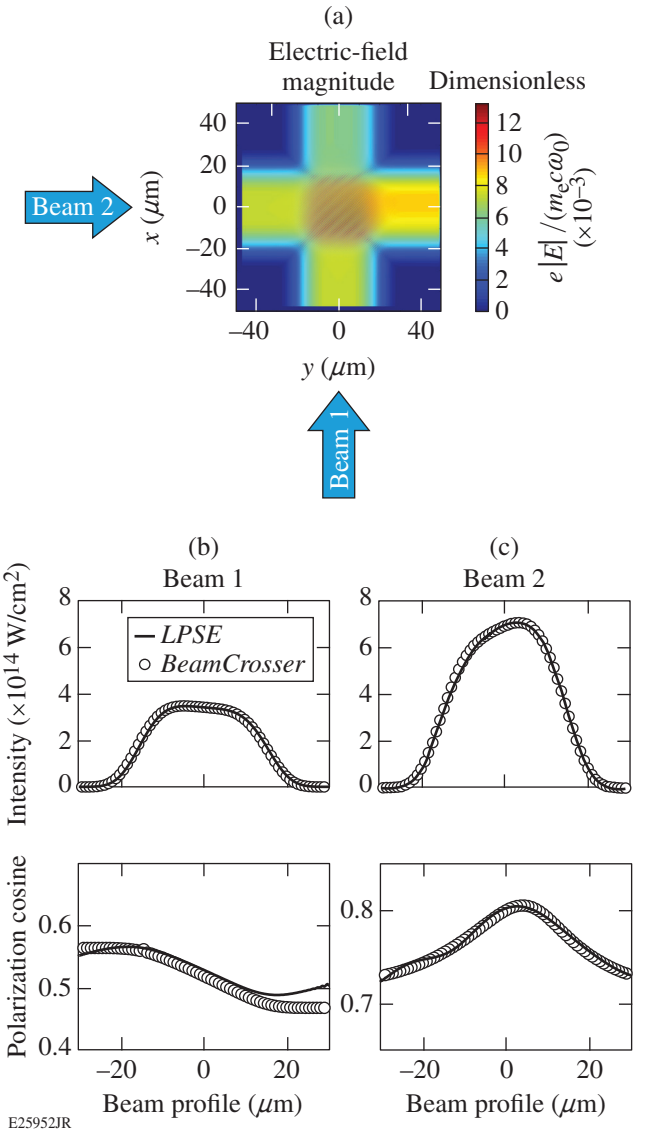

Figure 150.14
Laser-plasma simulation environment (*LPSE*) benchmarking: (a) *LPSE* simulation of the electric-field magnitude for two beams, both initially polarized 45° out of the plane, crossing in a plasma; (b) intensity profiles of the beams leaving the plasma for *LPSE* (solid curve) and *BeamCrosser* (circles); and (c) polarization cosine (where 0 is *s* polarized and 1 is *p* polarized) for the beams leaving the plasma from *LPSE* (solid curve) and *BeamCrosser* (circles) modeling.

ent in direct-drive implosions are missing from the ray-based models. Possible candidates for the missing phenomena include diffraction, polarization details, and nonlinear multibeam effects. All predictions presented here, unless mentioned otherwise, use a factor of $C_{CBET} = 2$.

Beam Coupling with No Wavelength Shift

In this section, the coupling between OMEGA beams during a direct-drive implosion is modeled when all beams are launched with the same wavelength (351 nm). It is important to note that although all beamlets enter the plasma with the same wavelength, the Doppler effect[56] changes the wavelength of each beamlet as it passes through the plasma. This wavelength shift varies across the beam profile depending on the path each beamlet takes through the coronal plasma. The magnitude of the Doppler shift is of the order of a few angstroms and must be included when calculating the CBET coupling along a beamlet.

All of the simulations use 1-D *LILAC* predictions with a nonlocal electron heat transport model of the coronal plasma conditions for a typical OMEGA symmetric direct-drive implosion of a CH target (shot 60,000). The plasma profiles were taken from a single time late in the pulse when CBET is predicted to be largest. Figure 150.15 shows the distribution of the 60 OMEGA laser beams. All beams use a super-Gaussian of the order of 4 (SG4) intensity profile measured for the SG4 distributed phase plates (DPP's) used in the implosion. All beams entered the plasma with 0.35 TW of power, which was the nominal power of all the beams in the implosion late in the pulse.

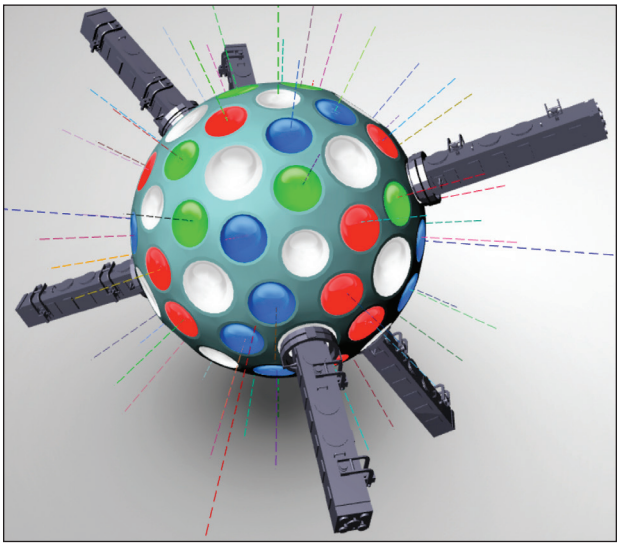

E26062JR

Figure 150.15
View of the OMEGA three-leg geometry: the beams fed by each of the three different beamline legs are shown in three different colors (red, green, and blue).

1. Two-Beam CBET Calculations

In a direct-drive implosion, each beam can interact with all other beams. In a nominally symmetric implosion, all beams have identical beam powers, intensity profiles, and relative geometries (i.e., the "view" from each beam looks the same with respect to the relative positions of the other beams). There is zero net exchange of total power between the beams, but there will still be a redistribution of power because of CBET. It is useful to determine which of the other beams has the strongest exchange with any single beam and the effect of that exchange on the effective beam intensity profile. How CBET affects the exchange between any two specific pairs of beams is mainly dependent on the angle between the two beams.

Figure 150.16 shows the laser absorption for two-beam simulations, where the angle θ between the beams was varied; $\theta = 180°$ indicates beams launched on opposing sides of the target. Because the coupling of any two beams is small compared to the total interaction between a set of 60 beams in an OMEGA symmetric implosion, a CBET multiplier of $C_{CBET} = 5$ was used for these two-beam interactions to accentuate the effects of CBET. The degradation in absorbed power is caused by redistribution of the beam power and is identical for both beams because of symmetry. The absorbed power is degraded most strongly by beams that are separated by 45° to 90°. Beams separated by more than 135° are practically decoupled. The absorption for these nearly opposite beams is essentially the same as when only intrabeam CBET interaction between a single beam and itself is considered. For 0° the beams are copropagating and the laser absorption is the same as the intrabeam CBET of a single beam with twice the intensity. Figure 150.16(b) shows the effective importance of CBET between beams at different angles. The effective importance in a direct-drive implosion depends on the number of beams at that angle. For an infinite number of beams, the importance of CBET for beams at a specific angle is determined by the change in absorption of the beam from Fig. 150.16(a) weighted by the differential surface area of a sphere for that angle ($\sin\theta \bullet d\theta$). The normalized change in absorption because of CBET weighted by $\sin\theta$ is shown by the solid red line in Fig. 150.16(b). Compared to Fig. 150.16(a), the importance of different beams is skewed toward the equator where the differential area is maximum. For a finite set of beams, the effect of CBET from one beam at a specific angle is weighted by the actual number of beams at that angle. The importance of different beams weighted for the symmetric 60-beam OMEGA geometry is shown by the

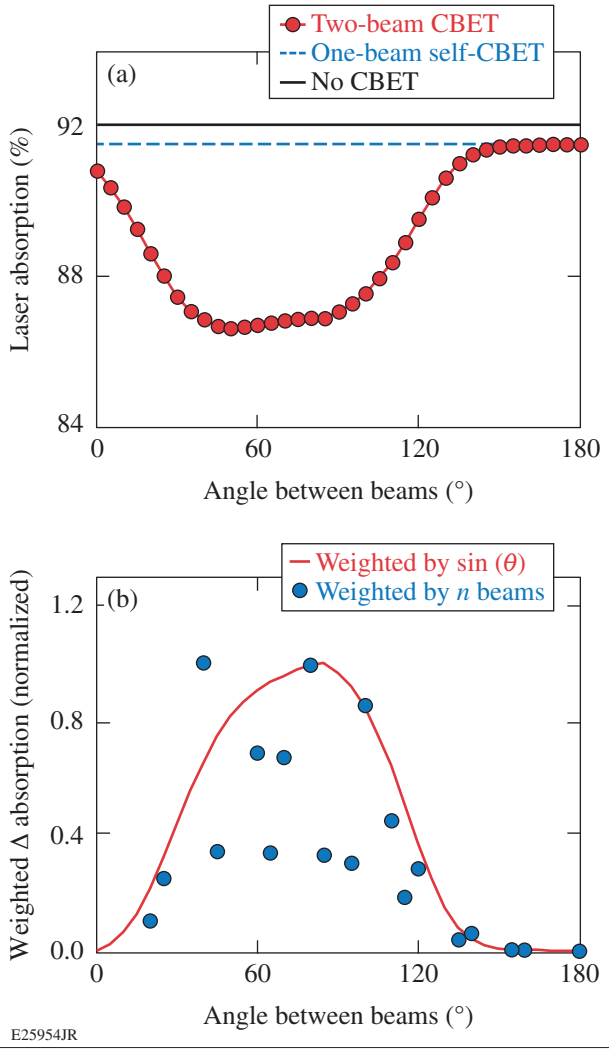

Figure 150.16
(a) Percent of laser power absorbed for two laser beams incident on an OMEGA symmetric implosion coronal plasma versus the angle between the launched beams. The black solid line is the laser absorption without CBET. The blue dashed line is the single-beam laser absorption with CBET calculated for intrabeam exchanges. (b) The change in absorption because of CBET weighted by the target surface area (red solid curve) and by the actual number of beams at specific angles for OMEGA (circles binned in 5° groups).

solid circles in Fig. 150.16(b). The largest effective change in absorption on OMEGA occurs from beams around 40°, 80°, and 100°.

Figure 150.17 shows the redistribution of power in the beam profile for two laser beams at a relative angle of 90°. Although CBET was known to shift the centroid of the outgoing beam profiles for simple beam geometries,[20,25] the redistribution is complicated for beams refracting through a spherical plasma where not all beamlets encounter a resonance with the other beam. Figure 150.17(a) shows the power gain and loss because of CBET integrated along the path of each beamlet (as described in **Ray Tracing and Model Gridding**, p. 63). The beamlets near the horizontal axis experience a net loss and those on the beam edge closest to the other beam experience a net gain. The total absorbed power in each beamlet is shown in Fig. 150.17(b). Near the beam center there is a region of lower absorbed power caused by the CBET losses. The overall absorption profile is radially asymmetric, and there is a shift in the centroid of the absorption away from the other beam compared to the no-CBET absorption profile [Fig. 150.17(c)].

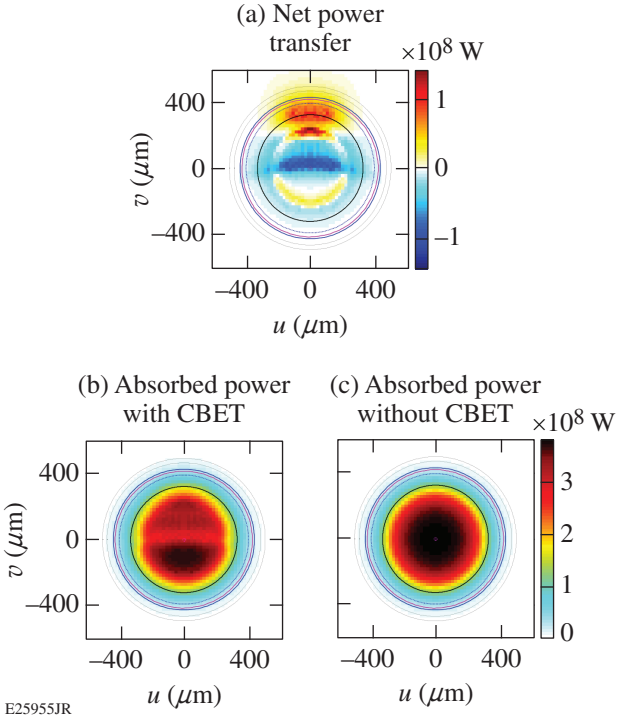

Figure 150.17
Beam profiles for the case of two beams at 90°. Profiles are oriented such that "up" is the directions of the other beam; i.e., the beamlets on the positive u direction are those that refract directly toward the other beam. (a) Power exchange caused by CBET summed along the full path of each beamlet. Red indicates a net gain while blue is a net loss. (b) Absorbed power summed along the full path of each beamlet; (c) absorbed power along the full path of each beamlet without CBET.

2. 60-beam CBET

Figure 150.18 shows the CBET exchange and absorption profiles calculated for the coronal plasma conditions modeled with the full 60 beams on OMEGA. In a direct-drive implosion, CBET's total effect on a beam is the sum of its interactions with all other beams. The absorbed power is significantly less in magnitude and shows a more-complicated profile structure than the two-beam case. As in the two-beam case, there is

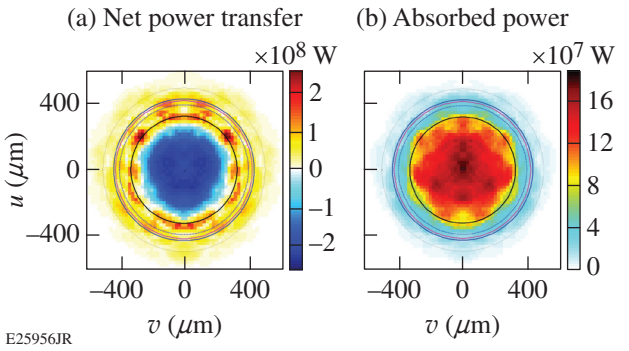

Figure 150.18
Beam profiles for CBET in the 60-beam OMEGA geometry. Profiles are oriented in such a way that "up" is the direction of the nearest-neighbor beam. (a) Power transfer because of CBET integrated along the path of each beamlet; (b) absorbed power integrated along the path of each beamlet.

no net exchange in power between beams because of beam symmetry but there is significant redistribution of power. The effect of many beams extends the ingoing losses over the hydrodynamically efficient small impact parameter beamlets and distributes the net outgoing gain to a ring of less hydrodynamically efficient high-impact parameter beamlets. The change in the absorbed power profile from the single-beam, no-CBET profile [Fig. 150.16(c)] has a significant effect on the absorption uniformity over the target surface.

Figure 150.19 shows an absorption surface map calculated by radially integrating the 3-D absorption at all points over the target surface. When CBET is ignored, the absorption is very uniform with an rms variation of ~0.2%. When CBET is included, the nonuniformity is an order-of-magnitude larger with an rms of 2.0%. Since there is no azimuthal symmetry in the absorption surface map, the effects of this nonuniformity cannot be captured by a 1-D or 2-D hydrodynamics code.

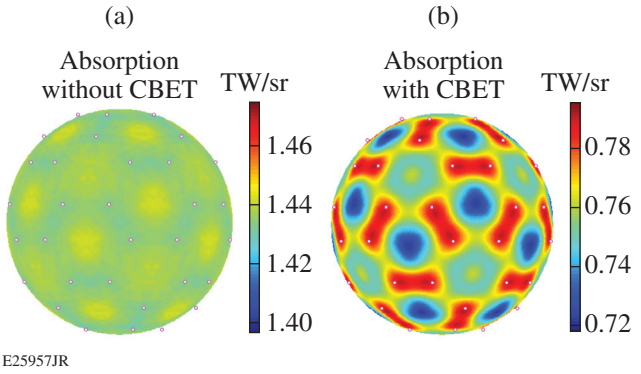

Figure 150.19
Surface map of the absorbed power over the target surface: (a) without CBET and (b) with CBET. The white dots show the positions of the beam centers.

CBET Mitigation Using Wavelength Detuning

One possible scheme for CBET mitigation during symmetric direct-drive implosions is wavelength detuning between groups of beams.[47] The 60 beams of the OMEGA Laser System originate from a single seed-pulse driver that is split three ways into "legs" and amplified separately to feed 20 beams each. The beams from each leg are distributed around the target chamber (Fig. 150.15). By shifting the wavelength of two of the legs in such a way that all three legs have different wavelengths, the CBET coupling between the groups of beams fed by the legs could be altered. With sufficient wavelength shifting, the groups of beams could be effectively decoupled from each other.

1. Single-Beam Wavelength Shift

Figure 150.20 shows the effect on absorbed laser power of shifting the wavelength of a single beam in a 60-beam symmetric implosion while keeping the other 59 beams fixed at 351 nm. The modeling predicts that small wavelength shifts can significantly increase or decrease the power absorbed in the single wavelength-shifted beam and that it takes a wavelength shift of $|\Delta\lambda| > 30$ Å to completely decouple the beam from the other 59 beams. The behavior shown in Fig. 150.20

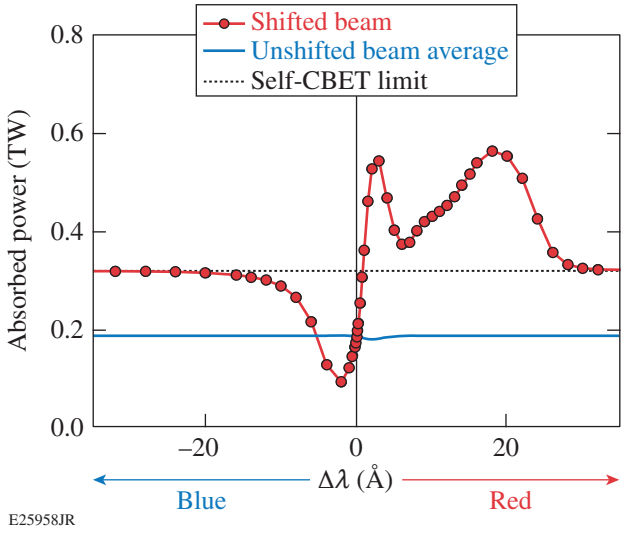

Figure 150.20
Absorbed power per beam in the OMEGA 60-beam geometry when one beam is wavelength shifted. The plot with red dots is the absorbed power in the single wavelength-shifted beam. The solid blue curve is the average absorbed power for the other 59 beams. The dotted black line is the absorbed power for a beam completely decoupled from all other beams but still experiencing CBET with itself.

is complicated because of the complex 3-D crossings with 59 other beams, but the behavior can be broken down into a few general phenomena.

When $\Delta\lambda$ is increased *negatively*, less Doppler shift is required to satisfy the IAW dispersion relation [Eq. (1)] for power loss in the central beamlets entering the plasma. This moves their resonance to smaller radii, where the plasma velocity is lower and the density is higher. Here the CBET coupling is stronger [Eq. (4)], increasing the losses compared to the $\Delta\lambda = 0$ case. At the same negative wavelength shift, the resonance for the power gain of the large-impact parameter beamlets moves radially outward, where the coupling parameter is weaker, thereby decreasing their power gain. Both effects reduce the total power absorption for the shifted beam, but the increased losses of the central beamlets are the primary source of the sharp drop in absorbed power shown in Fig. 150.20 as $\Delta\lambda$ is increased negatively. The absorbed power reaches a minimum at a shift of $\Delta\lambda \cong -2$ Å and then rises again as the resonance location for the power loss moves inside the beam shadow (Fig. 150.12) and CBET losses decrease until the beams decouple at $\Delta\lambda < -30$ Å. When $\Delta\lambda$ is increased *positively*, the resonance shifts are reversed, reducing the losses of the central beamlets, increasing the gains in the outer beamlets, and producing a sharp rise in the absorbed power that peaks near $\Delta\lambda \cong 3$ Å. Because the beam can gain energy from the 59 other beams, the total power absorbed from the shifted beam can exceed the original power in that beam (0.35 TW). For positive $\Delta\lambda$, a second maximum occurs near $\Delta\lambda \cong 18$ Å. This broad peak occurs because the wavelength shift is large enough to change the direction of CBET for the incoming central beamlets such that they gain energy while entering into the plasma from the other 59 beams.

2. Three-Leg Wavelength Shifts

Figure 150.21 shows the effect that shifting the wavelength of the three OMEGA legs has on the absorbed power and its uniformity over the implosion target for the coronal plasma conditions modeled. When $\Delta\lambda$ is given as the wavelength shift, it means that the beams in leg 1 are wavelength shifted by $-\Delta\lambda$ and those in leg 3 are shifted by $+\Delta\lambda$, while the beams in leg 2 remain unshifted at 351 nm. As $\Delta\lambda$ is increased from zero, CBET losses in leg 1 increase and the absorbed power in leg 1 beams drops, while the opposite occurs in leg 3, whose gains increase from CBET [Fig. 150.21(a)]. This loss/gain grows sharply until about $\Delta\lambda \cong 2$ Å. Here, the difference in absorbed power between legs 1 and 3 is maximum. As $\Delta\lambda$ is increased further, the CBET coupling between the legs decreases, and, as a result, the difference between their absorbed power decreases until $\Delta\lambda > 30$ Å, where the legs are essentially decoupled. If $\Delta\lambda$ is negative, these effects remain the same except the roles of leg 1 and leg 3 are reversed. Of particular interest is the region where $\Delta\lambda \cong 10$ Å. Here, the absorbed power averaged over all 60 beams is higher than the decoupled case ($\Delta\lambda > 30$ Å), indicating that CBET may work in favor of increased implosion drive.

Figure 150.21(b) shows that as $\Delta\lambda$ is increased from zero, the absorption nonuniformity (rms of the absorbed energy over the target surface) increases sharply to a maximum

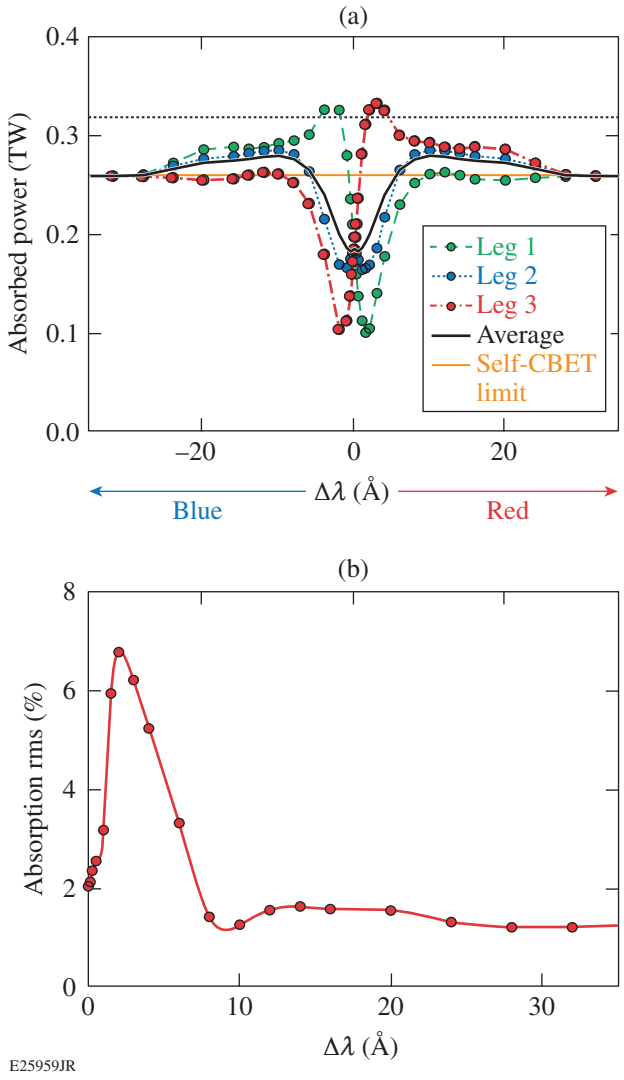

Figure 150.21
Effect of wavelength shifting the three legs (20 beams each) of the OMEGA 60-beam geometry on (a) the absorbed power per beam in each leg and (b) the root mean square (rms) of the absorbed energy over the target surface calculated by radially integrating the 3-D total absorption. Negative $\Delta\lambda$ shifts produce a reflection of Fig. 150.20(b) because of the symmetry shown in Fig. 150.20(a).

around $\Delta\lambda \cong 2$ Å, then falls as $\Delta\lambda$ continues to increase and the legs decouple. For $\Delta\lambda > 8$ Å, the absorption nonuniformity changes only weakly, but at the same location as the maximum total absorption ($\Delta\lambda \cong 10$ Å), there is a local minimum in the absorption nonuniformity of 1.3%, which is almost as small as the value when the legs are completely decoupled (1.2%). Figure 150.22 shows absorption surface maps calculated for wavelength shifts between the legs of 2 Å, 6 Å, and 10 Å. Not only does the total absorption rms change with $\Delta\lambda$, but the surface pattern of the nonuniformity varies as well.

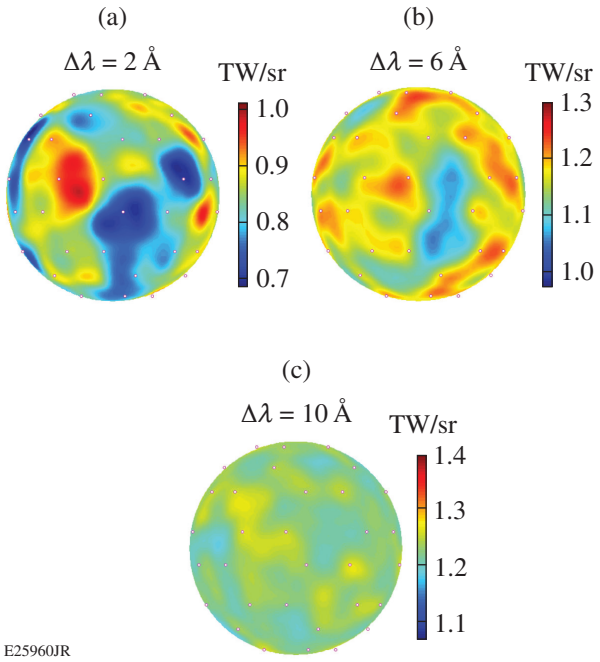

Figure 150.22
Nonuniformity of the absorbed power of the implosion target surface for (a) $\Delta\lambda$ = 2-Å rms = 6.8%; (b) $\Delta\lambda$ = 6-Å rms = 3.3%; and (c) $\Delta\lambda$ = 10-Å rms = 1.3%. Color bars for all three plots are set to cover similar magnitudes of rms variation.

Summary

A fully 3-D modeling of CBET for direct-drive symmetric implosions has been used to investigate the effects of wavelength detuning on CBET. The 3-D ray-based CBET model was benchmarked to full-wave calculations, providing confidence in the implementation of the model. For this study, coronal plasma conditions from late in the drive pulse of a typical warm OMEGA implosion were modeled. The model calculations show that beams with relative angles between 45° to 90° are most significant for CBET in OMEGA direct-drive implosions. The redistribution of laser power by CBET increases the absorption rms nonuniformity by an order of magnitude. Implosion degradation effects resulting from this increase in absorption nonuniformity from CBET should be studied by 3-D hydrodynamic modeling. By shifting the relative wavelengths of three groups of laser beams by ~10 Å, the total laser absorption was maximized and the rms absorption nonuniformity nearly minimized for these plasma conditions.

ACKNOWLEDGMENT

This material is based upon work supported by the Department of Energy National Nuclear Security Administration under Award Number DE-NA0001944, the University of Rochester, and the New York State Energy Research and Development Authority.

REFERENCES

1. J. Nuckolls et al., Nature **239**, 139 (1972).
2. R. S. Craxton, K. S. Anderson, T. R. Boehly, V. N. Goncharov, D. R. Harding, J. P. Knauer, R. L. McCrory, P. W. McKenty, D. D. Meyerhofer, J. F. Myatt, A. J. Schmitt, J. D. Sethian, R. W. Short, S. Skupsky, W. Theobald, W. L. Kruer, K. Tanaka, R. Betti, T. J. B. Collins, J. A. Delettrez, S. X. Hu, J. A. Marozas, A. V. Maximov, D. T. Michel, P. B. Radha, S. P. Regan, T. C. Sangster, W. Seka, A. A. Solodov, J. M. Soures, C. Stoeckl, and J. D. Zuegel, Phys. Plasmas **22**, 110501 (2015).
3. V. N. Goncharov, T. C. Sangster, T. R. Boehly, S. X. Hu, I. V. Igumenshchev, F. J. Marshall, R. L. McCrory, D. D. Meyerhofer, P. B. Radha, W. Seka, S. Skupsky, C. Stoeckl, D. T. Casey, J. A. Frenje, and R. D. Petrasso, Phys. Rev. Lett. **104**, 165001 (2010).
4. S. E. Bodner, D. G. Colombant, J. H. Gardner, R. H. Lehmberg, S. P. Obenschain, L. Phillips, A. J. Schmitt, J. D. Sethian, R. L. McCrory, W. Seka, C. P. Verdon, J. P. Knauer, B. B. Afeyan, and H. T. Powell, Phys. Plasmas **5**, 1901 (1998).
5. S. Skupsky and R. S. Craxton, Phys. Plasmas **6**, 2157 (1999).
6. J. H. Gardner and S. E. Bodner, Phys. Fluids **29**, 2672 (1986).
7. S. Skupsky and K. Lee, J. Appl. Phys. **54**, 3662 (1983).
8. I. M. Begg and R. A. Cairns, J. Phys. D: Appl. Phys. **9**, 2341 (1976).
9. C. J. Randall, J. J. Thomson, and K. G. Estabrook, Phys. Rev. Lett. **43**, 924 (1979).
10. R. W. Short and E. A. Williams, Phys. Rev. Lett. **47**, 337 (1981).
11. W. L. Kruer *et al.*, Phys. Plasmas **3**, 382 (1996).
12. J. F. Myatt, J. Zhang, R. W. Short, A. V. Maximov, W. Seka, D. H. Froula, D. H. Edgell, D. T. Michel, I. V. Igumenshchev, D. E. Hinkel, P. Michel, and J. D. Moody, Phys. Plasmas **21**, 055501 (2014).
13. R. K. Kirkwood *et al.*, Phys. Rev. Lett. **76**, 2065 (1996).
14. K. B. Wharton *et al.*, Phys. Rev. Lett. **81**, 2248 (1998).

15. K. B. Wharton *et al*., Phys. Plasmas **6**, 2144 (1999).
16. R. K. Kirkwood, J. D. Moody, A. B. Langdon, B. I. Cohen, E. A. Williams, M. R. Dorr, J. A. Hittinger, R. Berger, P. E. Young, L. J. Suter, L. Divol, S. H. Glenzer, O. L. Landen, and W. Seka, Phys. Rev. Lett. **89**, 215003 (2002).
17. W. Seka, H. A. Baldis, J. Fuchs, S. P. Regan, D. D. Meyerhofer, C. Stoeckl, B. Yaakobi, R. S. Craxton, and R. W. Short, Phys. Rev. Lett. **89**, 175002 (2002).
18. R. K. Kirkwood *et al*., Phys. Plasmas **12**, 112701 (2005).
19. C. J. McKinstrie *et al*., Phys. Plasmas **3**, 2686 (1996).
20. C. J. McKinstrie *et al*., Phys. Plasmas **5**, 1142 (1998).
21. H. A. Rose and S. Ghosal, Phys. Plasmas **5**, 1461 (1998).
22. J. A. F. Hittinger *et al*., J. Comput. Phys. **209**, 695 (2005).
23. J. D. Lindl *et al*., Phys. Plasmas **11**, 339 (2004).
24. P. Michel *et al*., Phys. Rev. Lett. **102**, 025004 (2009).
25. P. Michel *et al*., Phys. Plasmas **16**, 042702 (2009).
26. P. Michel *et al*., Phys. Plasmas **17**, 056305 (2010).
27. P. Michel *et al*., Phys. Rev. E **83**, 046409 (2011).
28. S. H. Glenzer *et al*., Science **327**, 1228 (2010).
29. E. L. Dewald *et al*., Phys. Rev. Lett. **111**, 235001 (2013).
30. J. D. Moody *et al*., Nat. Phys. **8**, 344 (2012).
31. G. D. Kerbel, Lawrence Livermore National Laboratory, Livermore, CA, Report UCRL-53101 (1981).
32. D. J. Strozzi *et al*., Phys. Rev. Lett. **118**, 025002 (2017).
33. M. M. Marinak *et al*., Phys. Plasmas **8**, 2275 (2001).
34. D. H. Edgell, W. Seka, J. A. Delettrez, R. S. Craxton, V. N. Goncharov, I. V. Igumenshchev, J. F. Myatt, A. V. Maximov, R. W. Short, T. C. Sangster, and R. E. Bahr, Bull. Am. Phys. Soc. **53**, 168 (2008).
35. W. Seka, D. H. Edgell, J. P. Knauer, J. F. Myatt, A. V. Maximov, R. W. Short, T. C. Sangster, C. Stoeckl, R. E. Bahr, R. S. Craxton, J. A. Delettrez, V. N. Goncharov, I. V. Igumenshchev, and D. Shvarts, Phys. Plasmas **15**, 056312 (2008).
36. I. V. Igumenshchev, D. H. Edgell, V. N. Goncharov, J. A. Delettrez, A. V. Maximov, J. F. Myatt, W. Seka, A. Shvydky, S. Skupsky, and C. Stoeckl, Phys. Plasmas **17**, 122708 (2010).
37. D. T. Michel, V. N. Goncharov, I. V. Igumenshchev, R. Epstein, and D. H. Froula, Phys. Rev. Lett. **111**, 245005 (2013).
38. C. J. Randall, J. R. Albritton, and J. J. Thomson, Phys. Fluids **24**, 1474 (1981).
39. D. H. Edgell, W. Seka, J. A. Delettrez, R. S. Craxton, V. N. Goncharov, I. V. Igumenshchev, J. F. Myatt, A. V. Maximov, R. W. Short, T. C. Sangster, and R. E. Bahr, Bull. Am. Phys. Soc. **54**, 145 (2009).
40. I. V. Igumenshchev, W. Seka, D. H. Edgell, D. T. Michel, D. H. Froula, V. N. Goncharov, R. S. Craxton, L. Divol, R. Epstein, R. Follett, J. H. Kelly, T. Z. Kosc, A. V. Maximov, R. L. McCrory, D. D. Meyerhofer, P. Michel, J. F. Myatt, T. C. Sangster, A. Shvydky, S. Skupsky, and C. Stoeckl, Phys. Plasmas **19**, 056314 (2012).
41. J. A. Marozas, T. J. B. Collins, D. H. Edgell, I. V. Igumenshchev, and J. F. Myatt, Bull. Am. Phys. Soc. **56**, 241 (2011).
42. J. Delettrez, R. Epstein, M. C. Richardson, P. A. Jaanimagi, and B. L. Henke, Phys. Rev. A **36**, 3926 (1987).
43. P. B. Radha, T. J. B. Collins, J. A. Delettrez, Y. Elbaz, R. Epstein, V. Yu. Glebov, V. N. Goncharov, R. L. Keck, J. P. Knauer, J. A. Marozas, F. J. Marshall, R. L. McCrory, P. W. McKenty, D. D. Meyerhofer, S. P. Regan, T. C. Sangster, W. Seka, D. Shvarts, S. Skupsky, Y. Srebro, and C. Stoeckl, Phys. Plasmas **12**, 056307 (2005).
44. D. H. Froula, I. V. Igumenshchev, D. T. Michel, D. H. Edgell, R. Follett, V. Yu. Glebov, V. N. Goncharov, J. Kwiatkowski, F. J. Marshall, P. B. Radha, W. Seka, C. Sorce, S. Stagnitto, C. Stoeckl, and T. C. Sangster, Phys. Rev. Lett. **108**, 125003 (2012
45. I. V. Igumenshchev, D. H. Froula, D. H. Edgell, V. N. Goncharov, T. J. Kessler, F. J. Marshall, R. L. McCrory, P. W. McKenty, D. D. Meyerhofer, D. T. Michel, T. C. Sangster, W. Seka, and S. Skupsky, Phys. Rev. Lett. **110**, 145001 (2013).
46. D. H. Froula, T. J. Kessler, I. V. Igumenshchev, R. Betti, V. N. Goncharov, H. Huang, S. X. Hu, E. Hill, J. H. Kelly, D. D. Meyerhofer, A. Shvydky, and J. D. Zuegel, Phys. Plasmas **20**, 082704 (2013).
47. J. A. Marozas, Laboratory for Laser Energetics, private communication (2017).
48. J. F. Myatt, J. G. Shaw, R. K. Follett, and D. H. Edgell, Bull. Am. Phys. Soc. **61**, BAPS.2016.DPP.UI3.4 (2016).
49. MATLAB® **R**2009**a**, The MathWorks Inc., Natick, MA 01760-2098 (http://www.mathworks.com).
50. D. H. Edgell, W. Seka, J. A. Delettrez, R. S. Craxton, V. N. Goncharov, I. V. Igumenshchev, J. Myatt, A. V. Maximov, R. W. Short, T. C. Sangster, and R. E. Bahr, Bull. Am. Phys. Soc. **52**, 195 (2007).
51. M. Born and E. Wolf, *Principles of Optics: Electromagnetic Theory of Propagation, Interference, and Diffraction of Light*, 7th expanded ed. (Cambridge University, Cambridge, England, 1999), pp. 752–758.
52. A. Sharma, D. V. Kumar, and A. K. Ghatak, Appl. Opt. **21**, 984 (1982).
53. L. Friedland and I. B. Bernstein, Phys. Rev. A **21**, 666 (1980).
54. Yu. A. Kravtsov and Yu. I. Orlov, Sov. Phys.-Usp. **26**, 1038 (1983).
55. W. L. Kruer, in *The Physics of Laser Plasma Interactions*, Frontiers in Physics, Vol. 73, edited by D. Pines (Westview, Boulder, CO, 2003), Chap. 4, p. 34.

56. T. Dewandre, J. R. Albritton, and E. A. Williams, Phys. Fluids **24**, 528 (1981).

57. W. L. Kruer, in *The Physics of Laser Plasma Interactions*, Frontiers in Physics, Vol. 73, edited by D. Pines (Westview, Boulder, CO, 2003).

58. A. K. Davis, D. Cao, D. T. Michel, M. Hohenberger, D. H. Edgell, R. Epstein, V. N. Goncharov, S. X. Hu, I. V. Igumenshchev, J. A. Marozas, A. V. Maximov, J. F. Myatt, P. B. Radha, S. P. Regan, T. C. Sangster, and D. H. Froula, Phys. Plasmas **23**, 056306 (2016).

59. J. Myatt, A. V. Maximov, W. Seka, R. S. Craxton, and R. W. Short, Phys. Plasmas **11**, 3394 (2004).

60. P. Michel *et al*., Phys. Plasmas **20**, 056308 (2013).

61. T. R. Boehly, R. L. McCrory, C. P. Verdon, W. Seka, S. J. Loucks, A. Babushkin, R. E. Bahr, R. Boni, D. K. Bradley, R. S. Craxton, J. A. Delettrez, W. R. Donaldson, R. Epstein, D. Harding, P. A. Jaanimagi, S. D. Jacobs, K. Kearney, R. L. Keck, J. H. Kelly, T. J. Kessler, R. L. Kremens, J. P. Knauer, D. J. Lonobile, L D. Lund, F. J. Marshall, P. W. McKenty, D. D. Meyerhofer, S. F. B. Morse, A. Okishev, S. Papernov, G. Pien, T. Safford, J. D. Schnittman, R. Short, M. J. Shoup III, M. Skeldon, S. Skupsky, A. W. Schmid, V. A. Smalyuk, D. J. Smith, J. M. Soures, M. Wittman, and B. Yaakobi, Fusion Eng. Des. **44**, 35 (1999).

62. P. Michel, L. Divol, D. Turnbull, and J. D Moody, Phys. Rev. Lett. **113**, 205001 (2014).